24. Phillips, M. M. *et al.* The reddening-free decline rate versus luminosity relationship for type Ia supernovae. *Astron. J.* **118,** 1766–1776 (1999).
25. Stritzinger, M. *et al.* Optical photometry of the type Ia SN 1999ee and the type Ib/c SN 1999ex in IC 5179. *Astron. J.* **124,** 2100–2117 (2002).
26. Hamuy, M. *et al.* The morphology of type Ia supernovae light curves. *Astron. J.* **112,** 2438–2447 (1996).

Supplementary Information accompanies the paper on **www.nature.com/nature**.

Acknowledgements All the co-authors participated in gathering the observations of the supernova. M.H. noticed the presence of hydrogen emission. M.M.P. noticed spectroscopic and photometric peculiarities and put forward the idea that these could be understood as due to SN/CSM interaction. N.B.S. provided the arguments about the progenitor types. M.H., M.M.P. and N.B.S. co-wrote this Letter. M.H. is a Hubble Fellow.

Competing interests statement The authors declare that they have no competing financial interests.

Correspondence and requests for materials should be addressed to M.H. (mhamuy@ociw.edu).

Ballistic carbon nanotube field-effect transistors

Ali Javey[1], Jing Guo[2], Qian Wang[1], Mark Lundstrom[2] & Hongjie Dai[1]

[1]*Department of Chemistry, Stanford University, California 94305, USA*
[2]*School of Electrical and Computer Engineering, Purdue University, West Lafayette, Indiana 47907, USA*

A common feature of the single-walled carbon-nanotube field-effect transistors fabricated to date has been the presence of a Schottky barrier at the nanotube–metal junctions[1–3]. These energy barriers severely limit transistor conductance in the 'ON' state, and reduce the current delivery capability—a key determinant of device performance. Here we show that contacting semiconducting single-walled nanotubes by palladium, a noble metal with high work function and good wetting interactions with nanotubes, greatly reduces or eliminates the barriers for transport through the valence band of nanotubes. *In situ* modification of the electrode work function by hydrogen is carried out to shed light on the nature of the contacts. With Pd contacts, the 'ON' states of semiconducting nanotubes can behave like ohmically contacted ballistic metallic tubes, exhibiting room-temperature conductance near the ballistic transport limit of $4e^2/h$ (refs 4–6), high current-carrying capability (~25 μA per tube), and Fabry–Perot interferences[5] at low temperatures. Under high voltage operation, the current saturation appears to be set by backscattering of the charge carriers by optical phonons. High-performance ballistic nanotube field-effect transistors with zero or slightly negative Schottky barriers are thus realized.

Transparent electrical contacts made to metallic single-walled carbon nanotubes (SWNTs) have revealed them to be ballistic conductors that exhibit two units of quantum conductance $4e^2/h$ ($R_Q = h/4e^2 = 6.5\,\mathrm{k\Omega}$)[4–6]. Carrier transport through the valence and conduction bands of a high-quality semiconducting SWNT could also be ballistic, presenting an opportunity to realize ballistic field-effect transistors (FETs) based on molecular electronic materials. However, such effort has been hampered by non-ideal electrical contacts made to semiconducting SWNTs. Previously, thermionic emission current and associated barriers between Ni contacts and SWNTs[7] have been reported for materials grown by chemical vapour deposition (CVD). Recently, significant Schottky barriers (SBs) have been found in SWNT-FETs (with Ti contacts and laser-oven nanotubes)[1–3]. Thermionic emission and tunnelling are involved in transport across the SBs, which limits the ON state conductance of nanotube FETs to be well below the $4e^2/h$ limit ($G_{ON} \approx 0.001 \times 4e^2/h$ for laser tubes[1–3]; and $G_{ON} \approx (0.05 - 0.3) \times 4e^2/h$ for CVD tubes[7–10]) at room temperature. At low temperatures, quenching of thermionic currents causes semiconducting SWNT devices to be about 10–100 times more resistive than at room temperature[7,11,12].

A solution is presented here to eliminate or greatly suppress SBs at metal–nanotube contacts. We find that for Pd-contacted, long, semiconducting SWNT devices (length $L = 3\,\mu\mathrm{m}$, diameter $d \approx 3\,\mathrm{nm}$, Fig. 1a) with back gates (SiO_2 thickness $t_{ox} = 500\,\mathrm{nm}$), the room-temperature ON state conductance through the valence band (VB) is up to $G_{ON} \approx 0.1 \times (4e^2/h)$ ($R_{ON} = 60\,\mathrm{k\Omega}$, Fig. 1b). For short channel nanotubes at room temperature ($L = 300\,\mathrm{nm}$, Fig. 1a), $G_{ON} = (0.4 - 0.5) \times (4e^2/h)$ ($R_{ON} = 13\,\mathrm{k\Omega}$, Fig. 1c). For long SWNTs, the ON state p-channel conductance exhibits metallic behaviour between room temperature and ~200 K, and typically shows a downturn in G_{ON} upon further cooling (Fig. 1b inset). The short nanotubes do not show such downturn, and the average G_{ON} monotonically increases as temperature T decreases to ~50 K (Fig. 1d), below which pronounced oscillations with Fabry-Perot type of interferences[5] appear in the G versus gate voltage (V_{gs}) data

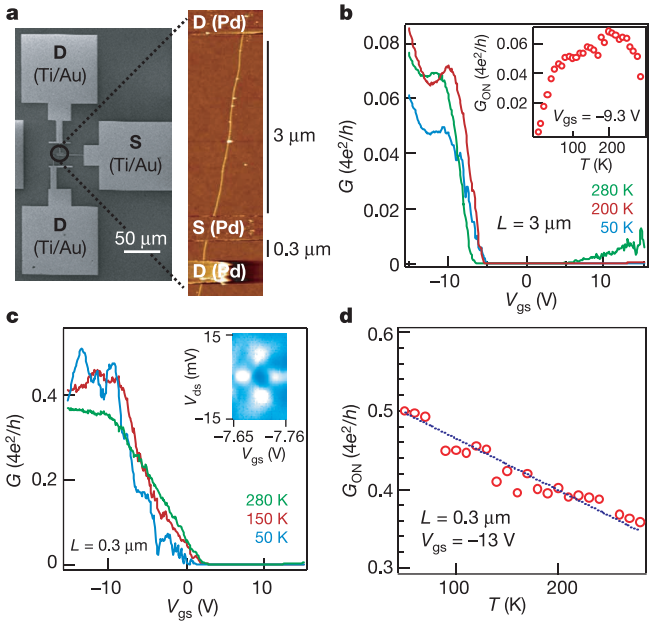

Figure 1 Pd-contacted long ($L = 3\,\mu\mathrm{m}$) and short ($L = 300\,\mathrm{nm}$) back-gated SWNT devices formed on the same nanotubes on SiO_2/Si. **a**, A scanning electron microscope (SEM) image (left) and atomic force microscope (AFM) image (right) of a representative device. CVD synthesis for SWNTs and device fabrication were as described previously[25,26], except that Pd was used to contact nanotubes. The catalyst used here gave a wide range of nanotube diameters (1.2 − 5 nm)[25]. Ti/Au metal bonding pads were used to connect to the Pd source (S) and drain (D) electrodes. (We note that Pd electrodes tended to be soft and not robust against electrical probing). The devices were annealed in Ar at 225 °C for 10 min after fabrication. The thickness of SiO_2 gate dielectric was $t_{ox} = 500\,\mathrm{nm}$, except for the devices in Fig. 4 with $t_{ox} = 67\,\mathrm{nm}$. AFM topographic height measurements were used to determine the diameters of SWNTs. The electrical data shown here were recorded with the devices placed in vacuum. **b**, G (at low S–D bias V_{ds}) versus gate voltage V_{gs} for a 3-μm-long SWNT ($d \approx 3.3\,\mathrm{nm}$) device recorded at various T. Inset, G_{ON} versus T for the device. **c**, G versus V_{gs} for a 300-nm-long tube section on the same tube as for **b** at various T. Differential conductance dI_{ds}/dV_{ds} versus V_{ds} and V_{gs} (inset, measured by a lock-in technique) at $T = 1.5\,\mathrm{K}$ shows a Fabry-Perot[5]-like interference pattern (bright peak $G \approx 4e^2/h$, dark region $G = 0.5 \times 4e^2/h$). Note that in certain V_{gs} regions, the pattern appears irregular, a phenomenon also seen for Fabry-Perot interference in metallic tubes[5]. **d**, G_{ON} versus T for the $L = 300\,\mathrm{nm}$ semiconducting tube down to ~50 K.

(peak conductance $\sim 4e^2/h$) (Fig. 1c inset). This corresponds to ballistic transport in the p-channel of semiconducting SWNTs. The metallic behaviour of the ON states of semiconducting SWNTs and G_{ON} approaching $4e^2/h$ strongly suggest nearly SB-free contacts made to nanotubes.

Because SBs are sensitive to the contact metal work function ϕ (ref. 1), we have carried out *in situ* modification of ϕ_{Pd} by utilizing the phenomenon that exposure of Pd to molecular hydrogen reduces its work function at room temperature[13]. Figure 2a shows that a SWNT-FET exhibits decreased p-channel conductance and increased n-channel conductance when exposed to H_2. This result is consistent with increased SB height for hole transport, and lowered barrier height for electron transport, due to reduced ϕ_{Pd} (ref. 1) caused by dissolved hydrogen[13]. The original pure Pd-contacted SWNT-FETs exhibit metallic behaviour for p-channel conduction (Fig. 2c), and highly linear conductance at low V_{ds} (Fig. 2d). After hydrogen modification of the Pd contacts, the p-channel of the device exhibits non-metallic behaviour (Fig. 2e), and inflection points (typical of SB-FETs) are observed in the $I_{ds} - V_{ds}$ characteristic of the device (Fig. 2f). These results suggest that higher SBs are formed to the p-channel of nanotubes with lower ϕ_{Pd} (Fig. 2b). The strong dependence of SB height on ϕ_{Pd} indicates the absence of appreciable interface states between SWNTs and Pd, and little or no Fermi level pinning[14]. We find that high-ϕ metal is not sufficient for forming transparent contacts to SWNT VBs. When experimenting with Pt with a high ϕ of 5.7 eV ($>\phi_{Pd} = 5.1$ eV), we find that Pt-contacted devices exhibit lower p-channel conductance and non-metallic behaviour for the ON states. This may be attributed to the poor sticking or wetting interaction between Pt and SWNTs, opposite to Pd (refs 15, 16). High-ϕ metal and high-quality metal–tube interfaces are thus both important for low contact barriers to the VBs of semiconducting nanotubes.

The transport properties of Pd-contacted SWNTs depend on nanotube diameter and length. For Pd-contacted SWNTs with $d \approx 1.7$ nm and $L \approx 275$ nm, $R_{ON} \approx 32\,k\Omega$ can be obtained (Fig. 3a inset). For SWNTs with $d < \sim 2$ nm, SBs at the Pd contacts are significantly low, but their elimination is more difficult (bandgaps of SWNTs $\propto 1/d$). Reducing the nanotube channel length from 3 μm to 300 nm always lowers R_{ON} by up to about 20 times, a trend observed for various diameter SWNTs (Fig. 3). Transport in

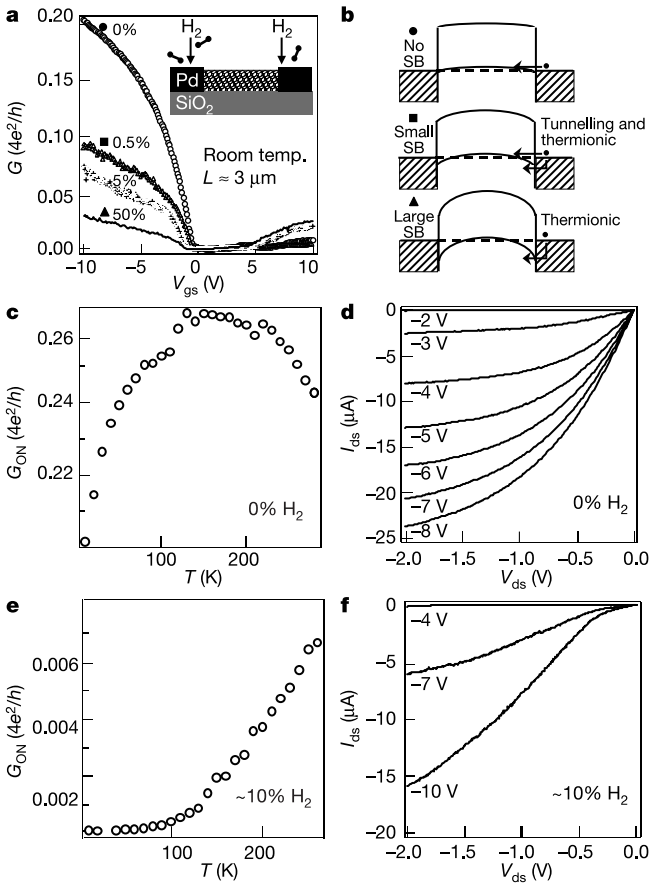

Figure 2 Properties of the metal/semiconducting-SWNT contacts as influenced by *in situ* metal work-function modification. **a**, Linear $G - V_{gs}$ for a SWNT-FET ($L = 3$ μm) before and after the pure Pd contacts were exposed to various concentrations of H_2. Note that no change in any of the device characteristics was observed for Ti/Au- and Mo-contacted tube FETs when exposed to hydrogen. **b**, Schematic ON state (for p-channel) band diagrams for the device under various H_2 concentrations, depicting the development of SBs to the valence band for higher [H_2] and lower ϕ_{Pd} (caused by dissolution of H_2 in Pd). The symbols in the diagrams (solid circle, square and triangle) correspond to those used in **a** to label the ON state gate voltages. **c**, G_{ON} versus T for the device with pure Pd contacts before exposure to H_2. **d**, $I_{ds} - V_{ds}$ curves for the device in **c** under various V_{gs} at room temperature. **e**, G_{ON} versus T for the same device as in **c** and **d** after exposure of the Pd electrodes to ~10% H_2. Both the p- and n- channel (data not shown) exhibit non-metallic behaviour, indicating mid-gap SBs to both valence and conduction bands with lowered ϕ_{Pd} by H_2. **f**, $I_{ds} - V_{ds}$ curves for the device in **e** under various V_{gs} at room temperature exhibiting typical SB-FET behaviour with inflection points in the curves. The plots in **d** and **f** clearly show the presence and absence of a SB in the two cases (with and without H_2 exposure) respectively.

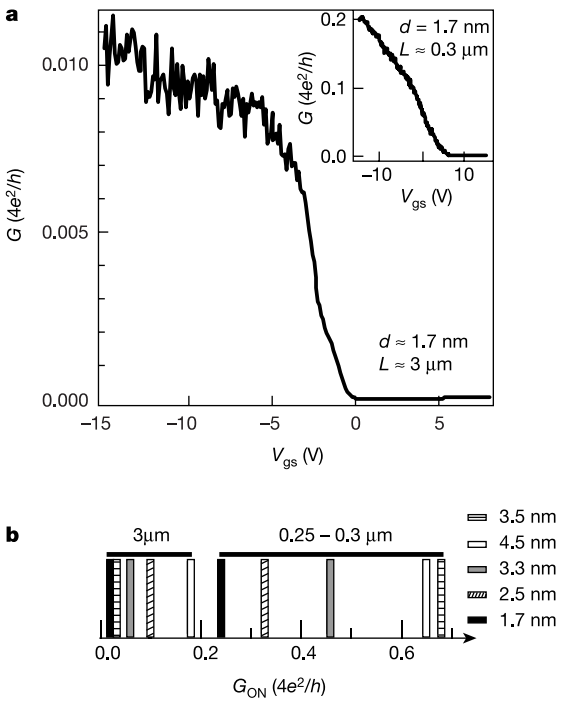

Figure 3 Geometry/transport-property relations for Pd-contacted semiconducting nanotubes. **a**, G versus V_{gs} for a $d \approx 1.7$ nm SWNT ($L = 3$ μm) contacted by Pd at room temperature. Inset, data for the same tube with $L = 275$ nm. **b**, G_{ON} for several $d \approx 1.5$ to 4.5 nm semiconducting SWNTs with lengths of ~300 nm and ~3 μm. Note that for our tube FETs with $t_{ox} = 500$ nm SiO_2 gate insulators, the threshold voltages (V_T) for the short devices tend to display a large shift (~5 V) to the more positive V_{gs} side from those of corresponding long devices (see **a** main panel versus **a** inset, and Fig. 1b versus Fig. 1c). This is attributed to the fact that the screening length in the quasi one-dimensional semiconducting nanotube devices is of the order of gate-dielectric thickness[27–29]. For short channels, this can lead to effectively p-doping of the nanotube ($L \approx 300$ nm $< t_{ox}$) and thus the V_T shift. Scaling of the gate dielectric for the current devices is essential to scale the screening length and to minimize the variation of V_T with channel length. Indeed, the short (~300 nm) and long (3 μm) Pd-contacted tube FETs with $t_{ox} = 67$ nm show only small V_T shift (<1 V, see Fig. 4a versus Fig. 4c, reproduced with over 30 such devices).

$L \approx 300$ nm tubes (of all diameters) is close to ballistic (R_{ON} down to $1.5 \times h/4e^2 \approx 10\,k\Omega$ at room temperature). Acoustic phonons (twistons) could account for the extra resistance[17], and quenching of these phonon modes at low T leads to G_{ON} approaching $4e^2/h$ and the observed metallic state, with clear manifestation of phase coherent resonances[6]. The higher R_{ON} for longer tubes suggests additional scattering along the length of long nanotubes. However, the precise nature of the scatters on the long semiconducting SWNTs is elusive, and could be due to structural defects, mechanical bending or chemical inhomogeneity. For long tubes, the upturn in the ON state resistance at low T is attributed to weak localization due to these defects, causing the deviation from metallic behaviour[17,18].

Figure 4 shows the detailed transistor data for long- and short-tube devices respectively with Pd contacts and back gates ($t_{ox} = 67$ nm for these FETs). Both devices exhibit $I_{ON}/I_{OFF} \approx 10^6$ (Fig. 4). The maximum 'on' state current reaches $I_{Dsat} \approx 25\,\mu A$ (current saturation at this level has been observed with metallic tubes previously[19]), about 4 times higher than achieved previously for CVD semiconducting tubes[9] (highest $I_{ON} \approx 4\,\mu A$ for SB tube FETs[12,20]). The current normalized by the width of the tube reaches $\sim 7{,}000\,\mu A\,\mu m^{-1}$. A key goal in transistor scaling is to maximize the saturation drain current for short channel and low voltage devices[21,22], and SB-free SWNT-FETs could be a promising approach to reach this goal. Negative SB-FETs will further enhance current delivery capability[21], and may be possible with nanotubes due to the lack of significant Fermi level pinning at the contacts (based on the current work and ref. 14).

We now turn to the issue of how the Pd-contacted nanotube transistors operate and compare them with SB-FETs[1–3] (operation involves gate modulation of the SB width) and metal-oxide-semiconductor FETs (MOSFETs[21,23], operation involves gate modulation of carrier density in the channel). For the ON states of our SWNT-FETs at room temperature, the short tubes can be considered as nearly ballistic channels ($R_{ON} = 10\,k\Omega$) while the long tubes are diffusive channels ($R_{ON} = 37\,k\Omega$). For the OFF states, the large $I_{ON}/I_{OFF} \approx 10^6$ suggests that large thermal activation barriers exist to limit the OFF state currents. In between the ON and OFF states, the subthreshold swing is $S \approx 150$ mV per decade for the long tube and $S \approx 170$ mV per decade for the short tube. The value of S is a sensitive function of different device geometry parameters, but the value observed here falls closer to the S versus ε/t_{ox} (ε is the dielectric constant) curve for MOSFETs than that for SB-FETs

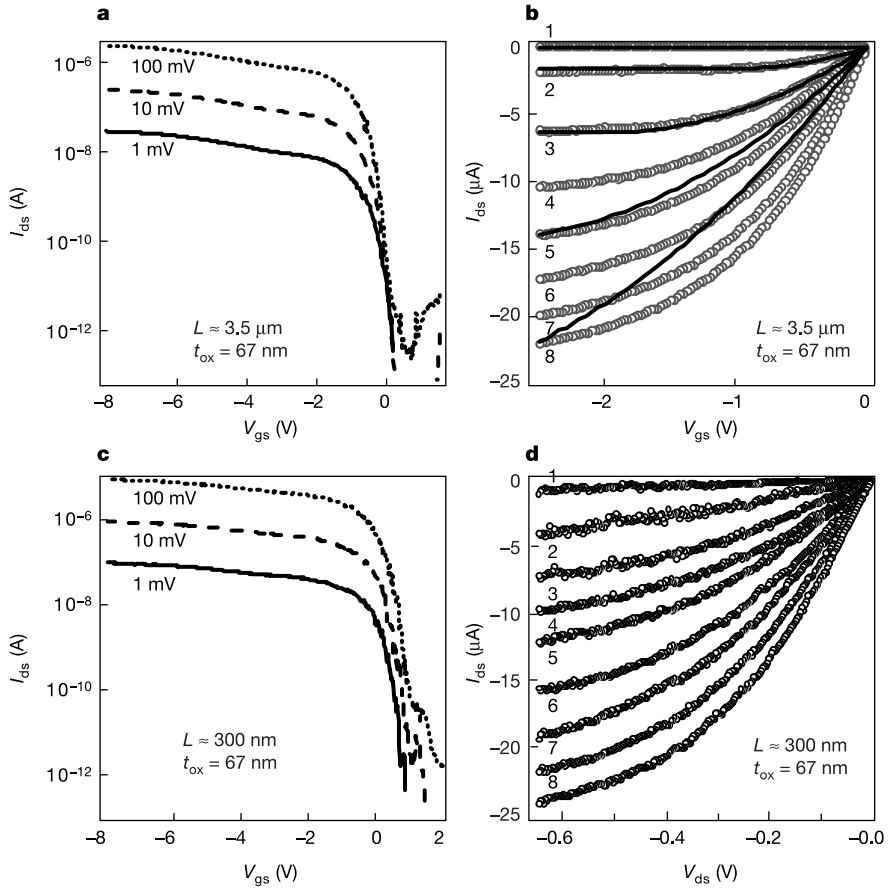

Figure 4 Room-temperature electrical properties of high-performance SWNT-FETs ($t_{ox} = 67$ nm). **a**, Transfer characteristics for a $d = 3.5$ nm and channel length $\sim 3\,\mu m$ SWNT with pure Pd contacts. $G_{ON} = 0.17 \times 4e^2/h$ ($R_{ON} \approx 37\,k\Omega$) under $V_{ds} = 1$ mV and $V_{gs} = -8$ V. **b**, $I_{ds} - V_{ds}$ versus V_{gs} for device in **a**. The curves (with circular symbols) labelled 1 to 8 correspond to $V_{gs} = -0.5$ to -7.5 V in steps of 1 V. The solid lines are calculated from the square-law model for MOSFETs to fit the experimental curves 1–5. **c**, Transfer characteristics for a device with channel length $L = 300$ nm formed on the same tube as in **a** and **b**. $G_{ON} = 0.65 \times 4e^2/h$ ($R_{ON} \approx 10\,k\Omega$) under $V_{ds} = 1$ mV and $V_{gs} = -8$ V. The current measured at $V_{ds} = 100$ mV for the OFF state is ~ 1 pA, as the hole current is limited by a body barrier in the valence band. The electron current, limited by a SB to the conduction band, must be less than 1 pA, and to limit electron current to such a small value, a SB height of ~ 0.35 eV is needed by simple analysis. Since the sum of the electron- and hole-barrier heights is the bandgap (~ 0.3 eV for this tube), a slight negative SB for the holes is found to be about -0.05 V. **d**, $I_{ds} - V_{ds}$ versus V_{gs} characteristics for the short tube device in **c**. The curves labelled 1 to 9 correspond to 0.5, 0, -0.5, -1, -1.5, -2.5, -3.5, -4.5 and -5.5 V, respectively. Note that the devices shown above were passivated by PMMA to eliminate hysteresis upon sweeping V_{gs} back and forth[30]. This allowed for more precise determinations of V_T. The devices in Fig. 3 were also passivated by PMMA.

(~800 mV per decade predicted for the SB case[2]). These results plus the high ON state conductance (G_{ON} up to $0.65 \times 4e^2/h$ at room temperature) strongly suggest SB-free MOSFET operation of nanotube transistors.

We have analysed the 3-μm-long tube FETs by using the MOSFET square-law model for diffusive transport[23] (the gate capacitance was obtained by solving the two-dimensional Poisson equation). The output characteristics can be well explained by the model for $V_{gs} \geq -2.5$ V (Fig. 4b with fit data in solid line) and a hole mobility of $\mu_h \approx 4{,}000\ cm^2\,V^{-1}\,s^{-1}$ is deduced. However, when the device is in highly ON states under $V_{gs} < -2.5$ V, we observe significant deviation of its characteristics from the square-law model (Fig. 4b) in the high-current regions of the $I_{ds} - V_{ds}$ curves. The saturation current I_{Dsat} (when $I_{Dsat} > 10\ \mu A$) grows slower than expected from the square-law model as more negative V_{gs} is applied, especially when I_{Dsat} approaches ~25 μA (Fig. 4b). Similar behaviour is well known for silicon MOSFETs when velocity saturation due to optical phonon scattering of high-energy carriers occurs, and the device changes from a square-law to linear dependence with gate voltage[23]. In light of the earlier observation that in metallic tubes, the current starts to saturate at ~10 μA and fully saturates at ~25 μA due to optical or zone-boundary phonon scattering[19], we suggest that a similar phenomena may be occurring at high currents (>~10 μA) in our nanotube FETs. That is, high current flows in 'turned-on' semiconducting nanotubes are also limited by optical phonon backscattering (this effect has not been observed in earlier tube FETs with maximum currents at ~7 μA; see, for example, refs 9 and 10). We expect that nanotube channel length scaling below the optical phonon scattering mean free path (~100 nm)[19] could lead to ballistic transport in the high-current regime, and further enhance the current delivery capability of nanotube FETs.

We have also analysed our short tube FETs by the square-law model, and found that the diffusive transport model completely fails to reproduce the device characteristics. This is an expected result, because transport in the short nanotubes is close to ballistic. Preliminary analysis based on a ballistic MOSFET model[10,24] leads to good but non-ideal fitting of the experimental data. Further theoretical work is needed to model the detailed behaviour of nanotube transistors near the ballistic transport regime. □

Received 19 April; accepted 2 June 2003; doi:10.1038/nature01797.

1. Heinze, S. *et al.* Carbon nanotubes as Schottky barrier transistors. *Phys. Rev. Lett.* **89,** 106801 (2002).
2. Appenzeller, J. *et al.* Field-modulated carrier transport in carbon nanotube transistors. *Phys. Rev. Lett.* **89,** 126801 (2002).
3. Heinze, S., Radosavljevic, M., Tersoff, J. & Avouris, P. Unexpected scaling of the performance of carbon nanotube transistors. Preprint at ⟨http://xxx.lanl.gov/cond-mat/0302175⟩ (2003).
4. White, C. T. & Todorov, T. N. Carbon nanotubes as long ballistic conductors. *Nature* **393,** 240–242 (1998).
5. Liang, W. *et al.* Fabry-Perot interference in a nanotube electron waveguide. *Nature* **411,** 665–669 (2001).
6. Kong, J. *et al.* Quantum interference and ballistic transmission in nanotube electron wave-guides. *Phys. Rev. Lett.* **87,** 106801 (2001).
7. Zhou, C., Kong, J. & Dai, H. Electrical measurements of individual semiconducting single-walled nanotubes of various diameters. *Appl. Phys. Lett.* **76,** 1597 (1999).
8. Rosenblatt, S. *et al.* High performance electrolyte gated carbon nanotube transistors. *Nano Lett.* **2,** 869–915 (2002).
9. Javey, A. *et al.* High-k dielectrics for advanced carbon-nanotube transistors and logic gates. *Nature Mater.* **1,** 241–246 (2002).
10. Guo, J. *et al.* Assessment of silicon MOS and carbon nanotube FET performance limits using a general theory of ballistic transistors. *IEE Int. Electron Devices Meeting Tech. Dig.* 711–714 (December 2002).
11. Javey, A., Shim, M. & Dai, H. J. Electrical properties and devices of large-diameter single-walled carbon nanotubes. *Appl. Phys. Lett.* **80,** 1064–1066 (2002).
12. Martel, R. *et al.* Ambipolar electrical transport in semiconducting single-wall carbon nanotubes. *Phys. Rev. Lett.* **87,** 256805 (2001).
13. Mandelis, A. & Christofides, C. *Physics, Chemistry and Technology of Solid State Gas Sensor Devices* (Wiley, New York, 1993).
14. Leonard, F. & Tersoff, J. Role of Fermi-level pinning in nanotube Schottky diodes. *Phys. Rev. Lett.* **84,** 4693–4696 (2000).
15. Zhang, Y., Franklin, N., Chen, R. & Dai, H. Metal coating on suspended carbon nanotubes and its implication to metal-tube interactions. *Chem. Phys. Lett.* **331,** 35–41 (2000).
16. Zhang, Y. & Dai, H. Formation of metal nanowires on suspended single-walled carbon nanotubes. *Appl. Phys. Lett.* **77,** 3015–3017 (2000).
17. Kane, C. L. *et al.* Temperature dependent resistivity of single wall carbon nanotubes. *Euro. Phys. Lett.* **6,** 683–688 (1998).
18. Fischer, J. E. *et al.* Metallic resistivity in crystalline ropes of single-wall carbon nanotubes. *Phys. Rev. B* **55,** R4921–R4924 (1997).
19. Yao, Z., Kane, C. L. & Dekker, C. High-field electrical transport in single-wall carbon nanotubes. *Phys. Rev. Lett.* **84,** 2941–2944 (2000).
20. Wind, S. J., Appenzeller, J., Martel, R., Derycke, V. & Avouris, P. Vertical scaling of carbon nanotube field-effect transistors using top gate electrodes. *Appl. Phys. Lett.* **80,** 3817–3819 (2002).
21. Guo, J. & Lundstrom, M. A Computational study of thin-body, double-gate, Schottky barrier MOSFETs. *IEEE Trans. Elec. Dev.* **49,** 1897–1902 (2002).
22. Guo, J., Lundstrom, M. & Datta, S. Performance projections for ballistic carbon nanotube field-effect transistors. *Appl. Phys. Lett.* **80,** 3192–3194 (2002).
23. Sze, S. M. *Physics of Semiconductor Devices* (Wiley, New York, 1981).
24. Rahman, A., Guo, J., Datta, S. & Lundstrom, M. Theory of ballistic nanotransistors. *IEEE Trans. Electron Dev.* and *IEEE Trans. Nanotechnol.* (Joint Special Issue on Nanoelectronics) (in the press).
25. Kong, J., Soh, H., Cassell, A., Quate, C. F. & Dai, H. Synthesis of individual single-walled carbon nanotubes on patterned silicon wafers. *Nature* **395,** 878–881 (1998).
26. Soh, H. *et al.* Integrated nanotube circuits: Controlled growth and ohmic contacting of single-walled carbon nanotubes. *Appl. Phys. Lett.* **75,** 627–629 (1999).
27. Odintsov, A. A. Schottky barriers in carbon nanotube heterojunctions. *Phys. Rev. Lett.* **85,** 150–153 (2000).
28. Leonard, F. & Tersoff, J. Novel length scales in nanotube devices. *Phys. Rev. Lett.* **83,** 5174–5177 (1999).
29. Nakanishi, T., Bachtold, A. & Dekker, C. Transport through the interface between a semiconducting carbon nanotube and a metal electrode. *Phys. Rev. B* **66,** 073307 (2002).
30. Kim, W. *et al.* Hysteresis caused by water molecules in carbon nanotube field effect transistors. *Nano Lett.* **3,** 193–198 (2003).

Acknowledgements We thank P. McEuen, W. Harrison, D. Antoniadis, J. Bokor and J. Tersoff for insights and sharing preprints/unpublished results, and D. Wang for SEM. The work at Stanford was supported by the MARCO MSD Focus Center, DARPA/Moletronics, SRC/AMD, and the Packard, Alfred Sloan and Dreyfus foundations. The work at Purdue was supported by the National Science Foundation Nanoscale Modeling and Simulation Program and by the Network for Computational Nanotechnology.

Competing interests statement The authors declare that they have no competing financial interests.

Correspondence and requests for materials should be addressed to H.D. (hdai@stanford.edu).

Low-loss hollow-core silica/air photonic bandgap fibre

Charlene M. Smith, Natesan Venkataraman, Michael T. Gallagher, Dirk Müller, James A. West, Nicholas F. Borrelli & Douglas C. Allan Karl W. Koch

Corning Incorporated, Sullivan Park, Corning, New York 14831, USA

Photonic bandgap structures use the principle of interference to reflect radiation. Reflection from photonic bandgap structures has been demonstrated in one, two and three dimensions and various applications have been proposed[1–4]. Early work in hollow-core photonic bandgap fibre technology[5] used a hexagonal structure surrounding the air core; this fibre was the first demonstration of light guided inside an air core of a photonic bandgap fibre. The potential benefits of guiding light in air derive from lower Rayleigh scattering, lower nonlinearity and lower transmission loss compared to conventional waveguides. In addition, these fibres offer a new platform for studying nonlinear optics in gases[6]. Owing largely to challenges in fabrication, the early air-core fibres were only available in short lengths, and so systematic studies of loss were not possible. More recently, longer lengths of fibre have become available[7,8] with reported losses of 1,000 dB km^{-1}. We report here the fabrication and characterization of long lengths of low attenuation photonic bandgap fibre. Attenuation of less than 30 dB km^{-1} over a wide transmission window is observed with minimum loss of 13 dB km^{-1} at 1,500 nm, measured on 100 m of fibre. Coupling between surface and core modes of the structure is identified as an important contributor to transmission loss in hollow-core photonic bandgap fibres.

We use a stack and draw method for the fabrication of photonic bandgap fibre (PBGF)[5,7]. In this process, a preform consisting of stacked capillaries is built and then reduced to an intermediate-